# The Effect of Ramp Location in a Strut Based Scramjet Combustor under non reacting flow field

# The Effect of Ramp Location in a Strut Based Scramjet Combustor under non reacting flow field

**A. Antony Athithan[1], S. Jeyakumar [1,2*] and R. Sivakumar[3]**

[1] Faculty of Engineering, Lincoln University College, Malaysia.
[2] Aeronautical Engineering, Kalasalingam Academy of Research and Education, India
[3] School of Mechanical Engineering, VIT University, Chennai, India

* sjeyakumar1974@gmail.com

**Abstract**. The scramjet engine is considered to be the high-speed propulsive system for hypersonic air-breathing vehicles. Researchers focus on various geometries of strut injectors to enhance the mixing and combustion efficiencies of the scramjet combustor. This paper reveals the non-reacting flow characteristics of various ramp locations in a scramjet combustor with strut injection. The ramps are symmetrically placed at three different locations upstream of the strut within the combustor. Air enters into the combustor inlet with Mach number 2, and the fuel is injected at the sonic velocity from the strut. The 2D supersonic flow characteristics are numerically investigated using ANSYS 18.0 software. The steady-state flow simulations are performed in this study. The flow field is modelled using RANS equations, and the k-ω SST turbulence model and default constants are chosen to investigate the flow characteristics within the combustor. The flow characteristics of the ramp based DLR scramjet combustors are compared with the baseline DLR scramjet model. The computational results are validated with the experimental data. The shock wave interaction from the ramps enhances the distribution of hydrogen in the lateral direction of the flow than the baseline strut configuration. The ramps create recirculation regions that could enhance fuel-air mixing. The ramp induced strut based DLR scramjet engine provides increased total pressure loss of the baseline DLR scramjet.

**Keywords**: Strut injection, ramp, hydrogen jet, computational fluid dynamics (CFD), scramjet, static pressure, total pressure loss.

## 1. Introduction

High-speed transportation depends on supersonic and hypersonic flights with a good understanding of fuel and air mixing performance inside the supersonic combustor is essential. Mixing of fuel with air and ignition and flame holding are the fundamental constrain in the design of the scramjet engine[1,2]. The main focus is on the fuel injection system because the fuel's residence time with air in the combustor is less than 1ms. Researchers have suggested different fuel injectors like flush wall injection[3–8], cavity-type injection[9–15], strut based injection[16–21], and their blends[22–27], etc., to augment mixing and flame holding techniques. The strut injectors of specific geometry enhance mixing and combustion efficiencies with optimum total pressure loss than other injection and flame holding configurations.

The experiments on strut based DLR scramjet combustor were conducted with a hydrogen fuel injection system by Waidmann et al.[28]. The numerical investigation on a two-dimensional scramjet combustor with a flamelet model [29] is validated with the reported experimental results of the DLT strut scramjet combustor. Kummitha et al. [30] investigated the supersonic combustor with an innovative design of strut injector, which involves the modified double arrow strut and rocket models shows. The results show that the impinging of the first oblique shock is created from the strut leading edge that is very small when compared to the basic strut. Thus, multiple reflections of shock waves help the fuel to mix early with the supersonic airstream. Rocket strut fuel injector causes high-pressure rise due to impingement of shock wave occurs at the same location. Consequently, the pressure downstream of the strut is high in rocket and double strut-type fuel injector when compared to basic strut. Due to the inclined fuel injector, the combustion efficiency is significantly higher in the case of both double and rocket strut models. Therefore, the decrease in ignition delay is noted in double and rocket strut models than basic DLR scramjet models.

The study conducted by Kumaran and Babu [31] numerically simulated the hydrogen-fueled supersonic combustor employing a multistep chemistry model and compared it with the single-step reaction model to evaluate the performance of the combustor. The study findings disclosed that a multistep chemistry model could be an exercise to evaluate the insight properties of the combustion reaction like heat release rate, ignition delay, etc. Conversely, the single-step model can offer better results for the combustor's overall performance with a decrease in computational cost. Gerlinger and Bruggemann [32] have studied the mixing of hydrogen jets supplied from a strut injector under cold supersonic airflow conditions. It is indicated that the thickness of mixing layerand the total pressure loss increases by raising the strut lip thickness that is mainly owing to the increased diffusivity of the hydrogen at the outer strut wall and the more robust shock wave formation. Huang et al. [33] executed the numerical simulation studies on hydrogen-air reaction mechanism, the injection pressure and temperature variations of a strut-type scramjet combustor. Their study proved that shocks are formed from the strut is pushed out of the duct with the subsonic flow for increasing the temperatures and injection pressure.

Choubey and Pandey [34] executed the numerical simulation analysis on two strut configuration in a scramjet combustor model by changing the strut's angle of attack and asserted that zero angles of attack make a surge in mixing and combustion efficiencies. There is another work by the researchers [20], and it deals with the effect of altering the strut geometry and orientation in the combustor from the inlet. Furthermore, it is disclosed that the optimum lip height and position of the strut functions in an essential role in improving the combustion efficiency. Three strut positioning in a scramjet combustor was computationally examined by Kumar et al. [35]. It was identified that the maximum combustion efficiency and thrust had been attained by Pareto-optimal optimization studies accordingly position the struts in the combustor.

The numerical study of Athithan A A et al. [40] on the effect of double ramp configurations in a strut based scramjet combustor shows the distribution of hydrogen is enhanced in the double ramp combustor along spatial direction than normal DLR strut combustor. The study concluded that deceleration of flow at downstream of the strut due to the shocks and its interactions from the double ramps and strut, furthermore leads to more ignition delay.

The above literature reveals the performance of strut based DLR combustor with various active methods. The effect of ramps in a strut based scramjet combustor is not detailed in the open literature. The present study influences the performance of wall-mounted ramps in a DLR scramjet model under a non-reacting steady supersonic field. The ramps are located at the bottom and top walls of the duct towards the upstream of the strut injector. The numerical investigation is carried out using the two dimensional RANS equation with k-ω SST turbulence model. The flow shock patterns and overall performance of the 2D combustor provide acceptable results as that of 3D analysis [39]. The effect of the ramps is accessed based on shock generation and interactions with the shear layers, wall pressures of the combustor, and the stagnation pressure loss.

## 2. Computational Method

### *2.1. Numerical Modelling*

The numerical studies of the scramjet model are accomplished by solving the two-dimensional momentum, mass, and energy conservative equations. In the current approach, the compressible Reynolds averaged Navier-Stokes equations (RANS) are solved with the SST k-ω turbulence model [36], which offers a good prediction of jet flows[37]. The flow governing equations [18] are discretized by the finite volume method framework of ANSYS18.0. The density-based solver with the implicit formulation and advection upstream splitting methods are adopted in this work [38]. The governing equations, i.e., mass, momentum, and energy equations written for the total enthalpy are expressed as:

Continuity equation

$$\frac{\partial \rho}{\partial t} + \frac{\partial}{\partial x_i}(\rho u_i) = 0 \tag{1}$$

Momentum equation

$$\frac{\partial}{\partial t}(\rho u_i) + \frac{\partial}{\partial x_i}\left(\rho u_i u_j\right) + \frac{\partial P}{\partial x_i} = \frac{\partial}{\partial x_i}\left(\tau_{ij}\right) \tag{2}$$

Energy equation

$$\frac{\partial}{\partial t}(\rho H) + \frac{\partial}{\partial x_i}(\rho H u_i) = -\frac{\partial}{\partial x_i}\left(\tau_{ij} u_i\right) + \frac{\partial q_i}{\partial x_i} \tag{3}$$

The turbulence kinetic energy, k, and the specific dissipation rate, ω is obtained from the following transport equations:

$$\frac{\partial}{\partial x_i}(\rho k u_i) = \frac{\partial}{\partial x_j}\left(\Gamma_k \frac{\partial k}{\partial x_j}\right) + G_k - Y_k + S_k \tag{4}$$

and

$$\frac{\partial}{\partial x_j}\left(\rho \omega u_j\right) = \frac{\partial}{\partial x_j}\left(\Gamma_\omega \frac{\partial \omega}{\partial x_j}\right) + G_\omega - Y_\omega + D_\omega + S_\omega \tag{5}$$

The terms, Gk represents the production of turbulent kinetic energy and Gω as the generation of ω, Γk and Γω represent the effective diffusivity of k and ω respectively, Yk and Yω represent the dissipation of k and ω due to turbulence, Dω represents the cross-diffusion terms and Sk and Sω as the user-defined source terms

### *2.2. The Computational domain*

Figure 1 shows the configuration of the supersonic model combustors that have been numerically investigated under non-reacting field using commercial code ANSYS 18.0. The channel has an inlet height of 50mm an inlet Mach number of 2.0 and an inlet static temperature of 300k. The DLR scramjet model experimented with by Waidmann [28] is shown in Figure 1. In the DLR scramjet combustor, a wedge-shaped strut is located at 77mm downstream of the combustor entrance and 25 mm away from the bottom wall. The strut has a length of 32mm and a height of 6mm. The hydrogen jet is injected through 15 orifices of 1.0mm in diameter. The ramps are placed at the bottom and top walls of the combustor at three axial locations, 77mm, 50mm, and 33mm from the combustor inlet and are denoted as Case 2, Case3, and Case 4, respectively. The ramp dimensions are also detailed in Figure 1, and the performance of the ramp locations in the strut type scramjet model is compared with the baseline DLR model (Case 1). The incoming air at the combustor inlet is at Mach number 2, and the hydrogen fuel is injected parallel to the airstream at the sonic condition. The flow is considered compressible and two dimensional. The operating conditions of the scramjet combustor are identical for all the cases.

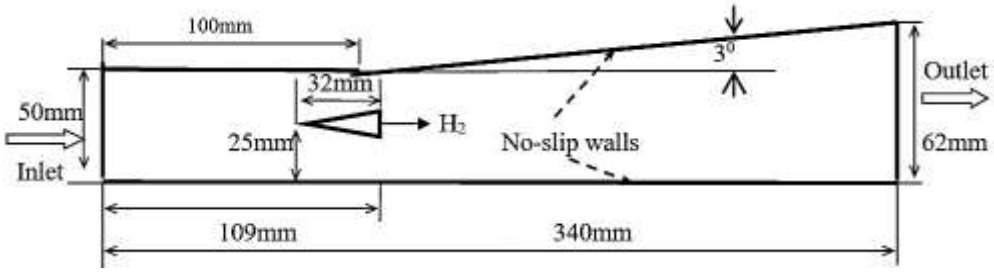


(a) Case 1

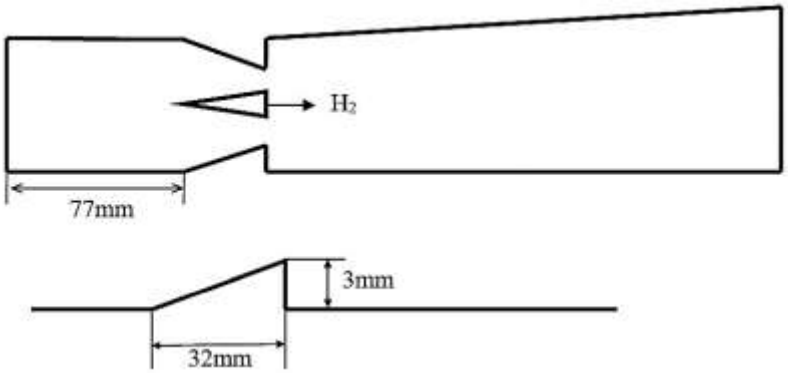


(b) Case 2

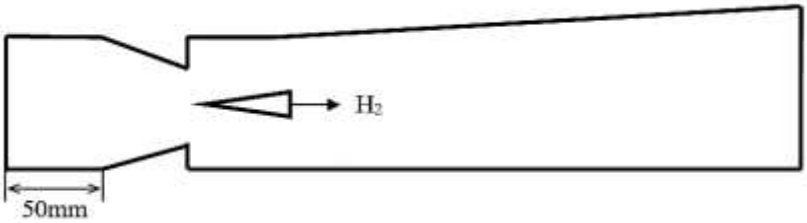


(c) Case 3

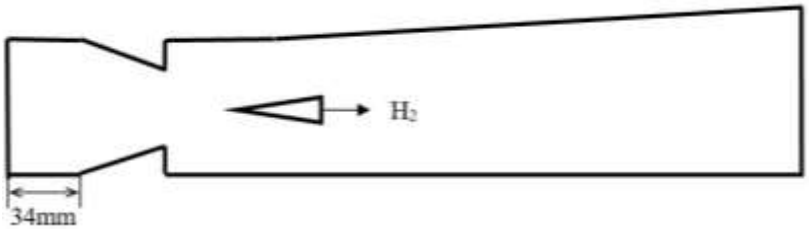


(d) Case 4

**Figure1.** Geometric details of scramjet Combustor for different configurations

*2.3. Boundary condition*

The boundary conditions are essential to solve the numerical governing equations. The air inlets are defined as supersonic conditions with specified variables of Mach number 2.0, and the hydrogen jet is injected from the strut at the sonic condition parallel to the flow direction. Dirichlet and Neumann boundary conditions are used as inlet and outlet boundary conditions, respectively. A fixed wall with

no-slip boundary condition is chosen for the walls of the combustor. The details of the inflow conditions are detailed in Table 1.

Table 1. Inflow conditions of air and fuel.

| Variable | Air | Hydrogen |
|---|---|---|
| Mach Number | 2 | 1 |
| Velocity (m/s) | 706 | 1240 |
| Temperature(K) | 340 | 250 |
| Pressure (bar) | 1.0 | 1.0 |
| Density (kg/m$^3$) | 1.002 | 0.097 |
| Mass fraction of $O_2$ | 0.232 | 0 |
| Mass fraction of $H_2$ | 0 | 1 |
| Mass fraction of $H_2O$ | 0.032 | 0 |

*2.4. Grid independence study*

The numerical solution accuracy to the problem mainly depends on grid size, hence for this investigation grid independence study has been performed. Three different grids, namely coarse (146146), medium (191607), and fine (290112) meshes, are employed to optimize the grid resolution for the convergence analysis. For the entire flow field, the y+ value is less than 1.0 (6.1e-7), which corresponds to the first-row cell height specified at 0.001 mm. Figure 4 shows the grid independence study, and it is found that the distribution of static pressure at the combustor's bottom wall for all the mesh size shows the variance of less than 1%. The medium and fine meshes show the same result, hence to reduce the computational time, the medium-sized mesh is considered for the analysis. The convergence criteria for the numerical simulation is considered based on the variation of the net mass flux of the flow across the combustor falls below 0.001kg/s, i.e., is less than 0.1% of the fuel mass flow.

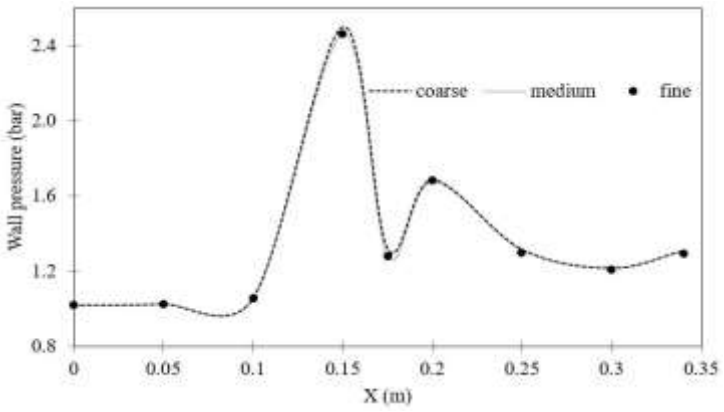


**Figure 2.** Grid independence study

## 3. Validation

The computational study is validated with the experimental results of Waidmann et al. [28] in terms of shadowgraph image and wall pressure plot and is shown in Figures 3 and 4, respectively. The inflow conditions for the experimental and numerical investigations are identical. The inlet flow to the combustor is Ma=2.0. The inflow parameters are presented in Table 1. The numerical result shows the shock generated from the strut, jet stream from the injector, and shock reflection pattern from the combustor wall is similar to that of the experimental result. The wall static pressure values at the

bottom wall of the DLR scramjet model are presented in figure 4 for the validation at the steady-state condition. The simulation results of the wall static pressures along the axis are well-matched with the experiment result are shown in figure 4. The maximum wall static pressure is observed at X = 0.12m, for both experimental and numerical studies. It is noted that numerical results are in qualitative agreement with the experimental results of the reference [28].

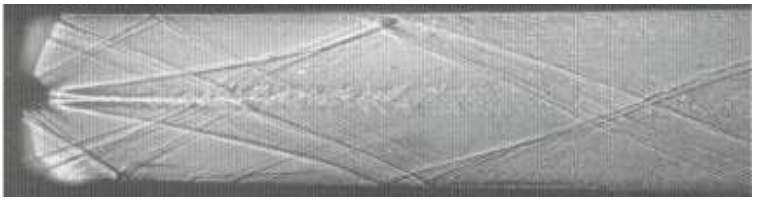

(a) Experimental Shadowgraph

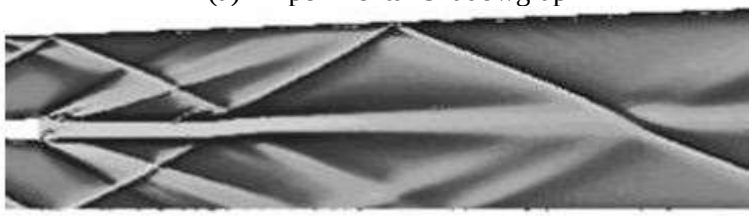

(b) Numerical shadowgraph

**Figure 3.** Comparison of (a) Experiment result with (b) numerical simulation

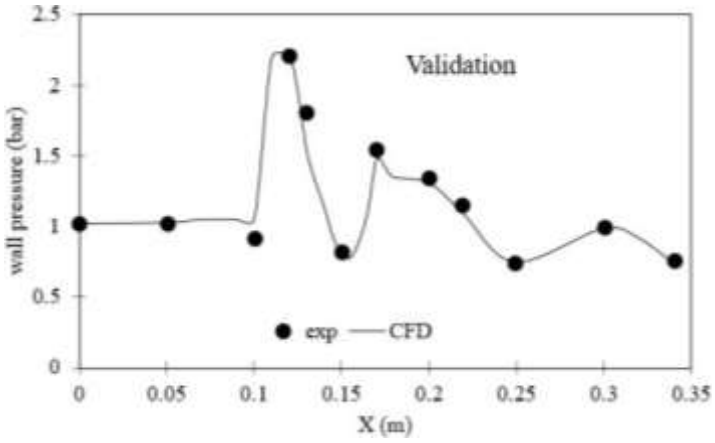


**Figure 4.** Validation of wall static pressure with experimental results

## 4. Result and discussion

The numerical investigations on the flow characteristics of ramps positioned on the top and bottom walls of a DLR scramjet combustor under a non-reacting flow field are discussed and compared with the typical DLR model. Figure 5 shows the shadowgraph images of the different geometry profiles that provide the details about the shocks and shear layer patterns inside the duct. The leading edge oblique shock waves from the strut in the scramjet combustor undergo multiple shock reflections from the combustor walls that are observed from Case 1. These reflected shock waves interact with the trailing edge shock from the strut and impinge on the fuel stream shear layer. For case 2, additional shockwaves are observed at the leading edge of the ramps that interact with the oblique shock wave emanated from the strut that decelerates the flow downstream. The shock waves emanated from the trailing edges of the ramps and strut interact with the fuel stream downstream that may enhance mixing of the fuel-air stream downstream with the lesser supersonic stream than the case 1. The ramp related shocks interact with leading-edge shock from strut upstream of strut injector as the ramps are

located upstream of the strut (case 3). These reflected shocks from the internal walls of the combustor overlap at different locations downstream of the strut with lesser intensity than case 2. In case 4, the ramp-related shock from the leading edge of ramps interacts upstream of the strut, and the leading edge shock waves from the strut impinge the trailing edge shocks of the ramp which results in deceleration of the flow downstream of the strut. Moreover, the upstream positioning of ramps creates the flow separation downstream of the ramp base due to the shock boundary layer interactions. The shock interactions and the flow separations in the supersonic flow field are perceived from Figure 6.

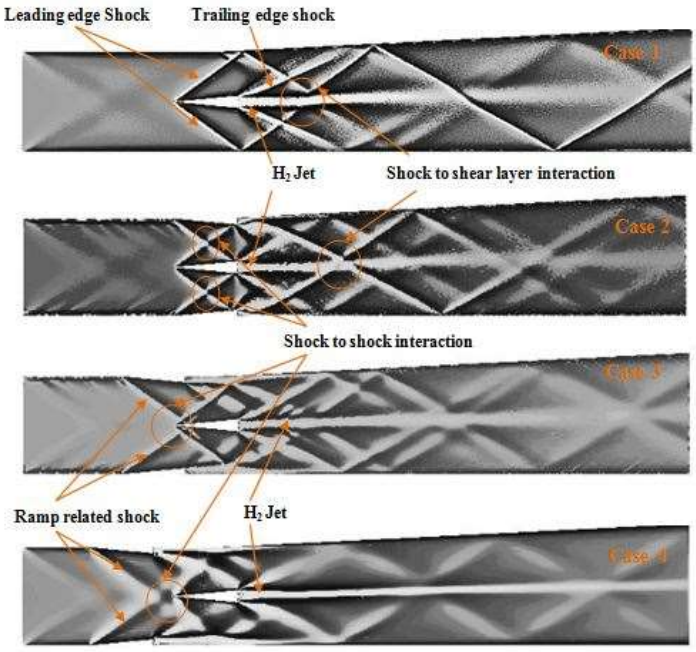


**Figure 5.** Shadowgraph image of combustor model with ramps at the bottom and top wall of duct in different positions

Figure 6 shows the Mach number contour comparison of different scramjet combustor profile. It is seen that the oblique shock waves are created at the leading edge of the strut, which gets reflected into the strut from the bottom and top wall of the combustor. The flow separations are observed downstream of the ramps due to the shock boundary layer interactions. The flow separation increases as the ramps are moved toward the combustor inlet. The recirculation regions are formed at the trailing edge of ramps, and these recirculation regions will act as flame holders and enhance fuel-air mixing. Figure 7 shows the recirculation region formed inside the combustors. For case 1, small vortices are noticed near the trailing edge of the strut. However, for case 2, 3 and 4, the additional recirculation regions are formed near the top and bottom wall of ramps. The large vortices are observed downstream of the ramps for case 3 compared to other ramp cases. It is well known that recirculation will be formed at the downstream of a ramp or a backward facing step in a supersonic flow field. For case 3, the shock boundary layer interaction at the base of the ramps creates a flow separation downstream of the ramp. The flow separation regime is comparatively larger for case 3 compared to the other cases where the recirculation region is formed through the separation region.

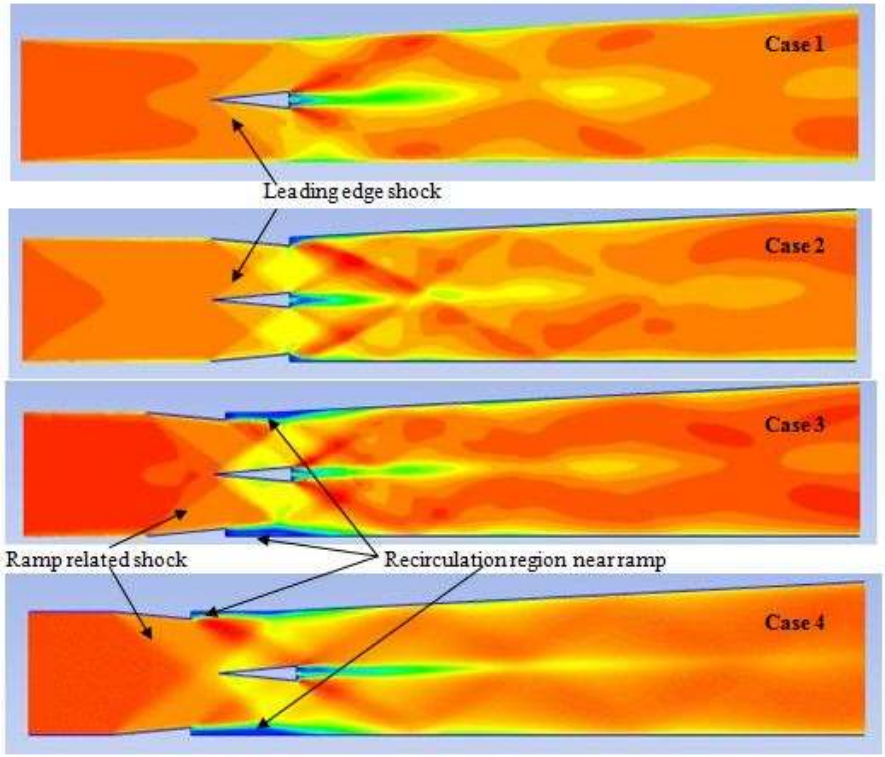


**Figure 6.** Mach number contour comparison of scramjet combustor with strut ramp at different position

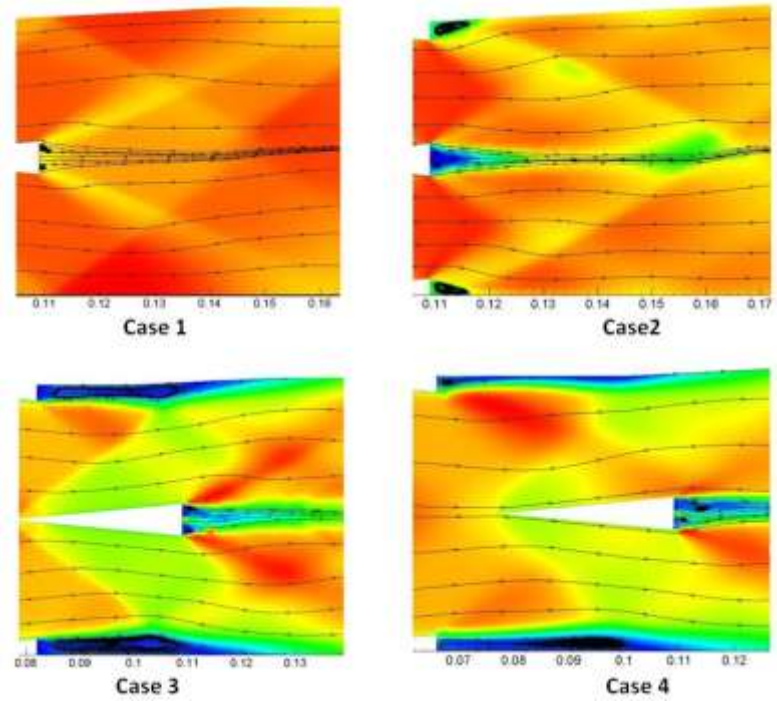


**Figure 7.** Streamline for various axial locations of the ramps in the DLR scramjet model

*4.1. Wall static pressure*

The wall pressure variations along the bottom wall and centreline of the combustor are shown in

Figure 8 (a, b). The wall pressure distribution is uniform for the typical DLR scramjet model till x=0.1m, subsequently, a wavy pressure profile is noted. The wavy nature of the pressure profile is due to the shock waves generated from the strut edges and its reflections from the combustor walls. An increase in static pressure profiles is observed for case 2 and case 3 from x = 0.05m due to the shock generated from the edges of the ramps. A peak pressure value is observed for case 4, at x = 0.1m due to the shock interactions and flow separation, which creates a compressive zone till the strut injection regime. It is notable that maximum static pressure from the bottom wall and midline of the duct at point x=0.1m to 0.15m, respectively. It is due to the intense shock wave reflections and flow separations inside the combustor.

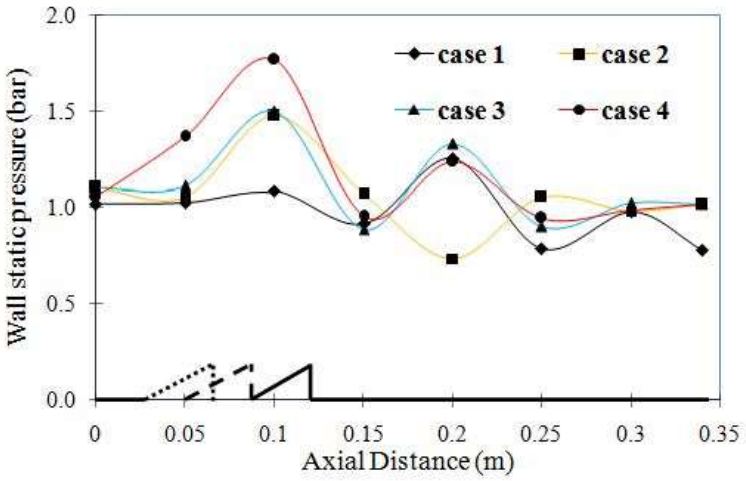


(a)

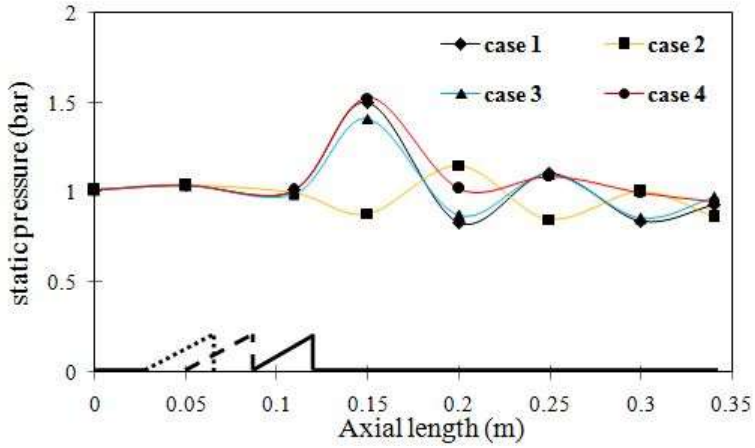


(b)

**Figure 8.** Pressure variation at (a) bottom wall and (b) centreline of the combustor

*4.2. Mass fraction of $H_2$*

The hydrogen mass fraction distribution at the three axial locations viz, X=0.15m, 0.2m, and 0.275m across the combustor are shown in Figure 9. At X = 0.15m, the distribution of hydrogen in the spatial direction is enhanced for case 2 than other configurations that may improve the combustion zone. Case 1 and case 4 show higher hydrogen mass fraction at X=0.2m, indicates that the shock waves' interaction with the fuel stream is less intense than case 2 and case 3. The hydrogen mass fraction is almost uniform for all the cases at X = 0.275 m, indicating that the fuel-air stream mixing is identical for all the configurations. The distribution of hydrogen near the walls of the combustor is negligible

for all the cases. Further investigations on the reacting flow studies will reveal the effectiveness of the mixing and hydrogen distribution in the scramjet combustor.

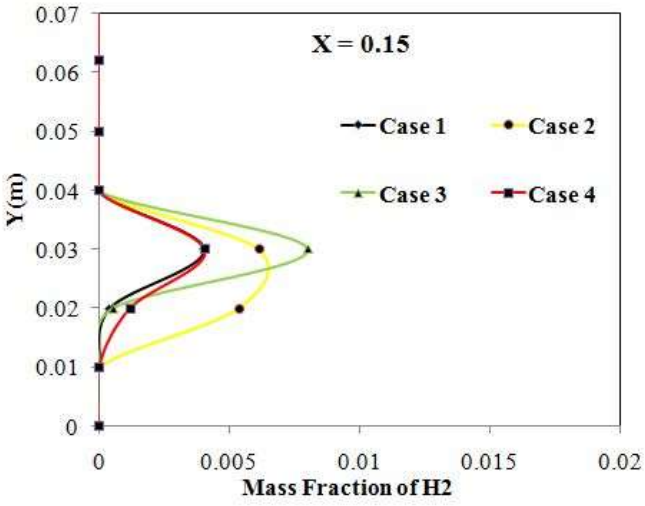


(a)

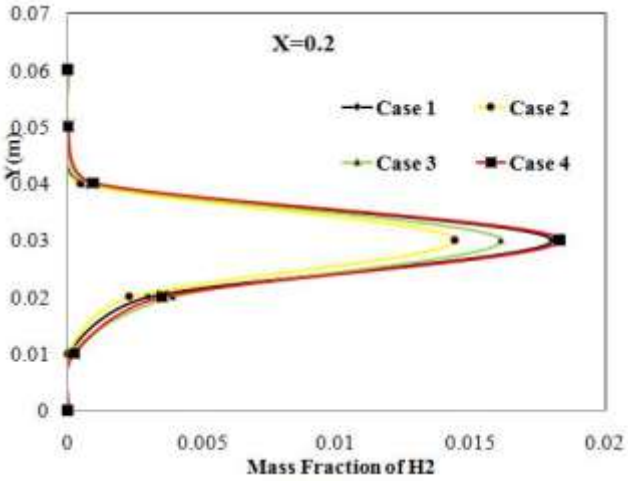


(b)

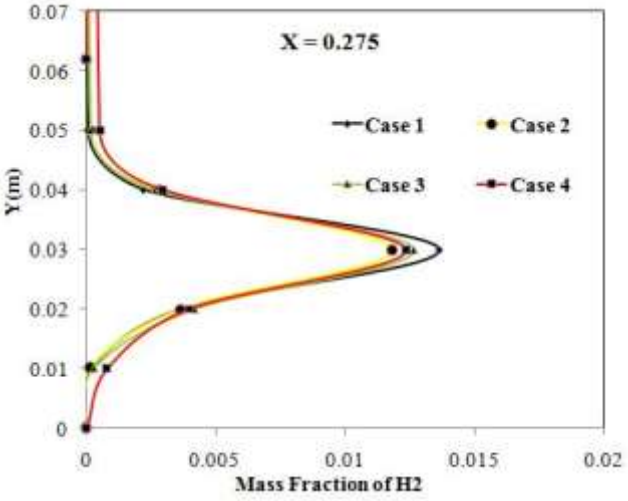


(c)

**Figure 9.** Mass fraction of hydrogen at (a) X=0.15m (b) X=0.2m and (c) X=0.275m.

*4.3. Total pressure loss*

The process of mixing with the shock waves is the irreversible process and causes the generation of entropy with total pressure losses. Generally, the more pressure losses occurs with an increase in mixing enhancement due to more oblique shock waves than other cases and their interaction with the shear mixing layer. The total pressure loss is calculated as,

$$\eta_t = 1 - \frac{\int_A P_o \rho_u dA}{\int_A P_{oinl} \rho_u dA} \quad (4)$$

Figure 12 shows the total pressure loss across the combustor at different locations. The higher pressure loss is noticed for the combustor with double ramps, due to the more shock wave interactions which decelerate the flow downstream and enhances total pressure loss compared to the DLR scramjet model (case1). It is observed that the maximum pressure loss of about 18% is observed for case 4 due to the shock waves interaction upstream of the strut, shock boundary layer interaction and flow separations create a compressive zone that decelerates the flow to the low supersonic condition compared to other ramp cases. For case 1, the total pressure loss of about 7%, which is comparatively lower than other cases with double ramps.

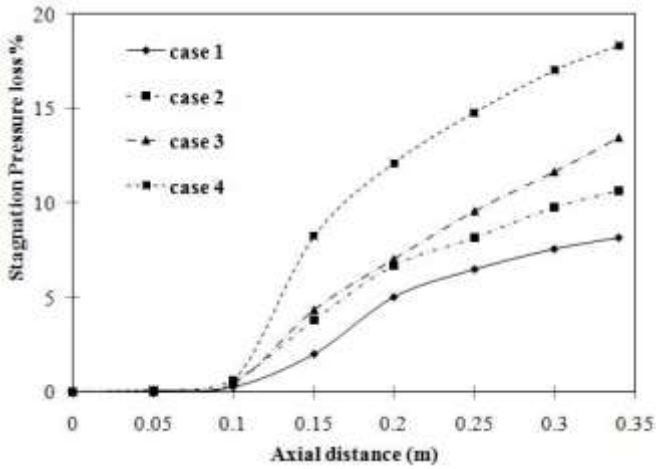


**Figure 10.** Total pressure loss for various geometry profile of the combustor

## 5. Conclusion

The numerical investigations of the normal DLR strut type scramjet combustor with upstream double ramps at the bottom and top walls of the combustor duct are carried out with non-reacting flow field conditions using the RANS equation. The effectiveness of the ramps locations along with the strut injection is analyzed based on the key parameters, such as wall static pressures, hydrogen mass fraction at various cross-sections, and total pressure loss across the combustor. The numerical results are validated with the reported experimental data, which shows higher correlations. The shadowgraph images show that more shock is formed for the double ramp DLR combustor than the typical DLR combustor model.

- The shock boundary layer interactions and flow separation resulting in higher wall static pressure for case 4 are compared to other double ramp profiles.
- The hydrogen distribution near the strut injector region enhances in the lateral direction as the ramps are positioned towards the combustor inlet.
- The shockwaves from the ramps decelerate the supersonic airflow downstream of the strut compared with the DLR scramjet model.

- In addition, more recirculation regions are formed for a double ramp combustor profile than the DLR scramjet model that acts as flame holders.
- The total pressure loss of the flow increases compared to the baseline scramjet model due to the more shock waves interaction arises from the ramps. The reacting flow studies will reveal the effectiveness of ramps in the strut based combustor is considered for future investigations.

## Appendix

Nomenclature

| | |
|---|---|
| Ma | Mach number |
| Po | total pressure |
| P | Static pressure |
| ρ | density |
| u | velocity |
| $\dot{m}$ | mass flow rate |
| k | turbulence kinetic energy |
| ω | specific dissipation rate |
| $G_k$ | production of turbulent kinetic energy |
| $G_\omega$ | generation of ω |
| $\Gamma_k$ and $\Gamma_\omega$ | effective diffusivity of k and ω |
| $Y_k$ and $Y_\omega$ | dissipation of k and ω |
| $D_\omega$ | cross-diffusion terms |

## References

[1] J. Kurian, K.. Habeeb, Cavities for Thermal and Momentum Mixing of Dual Supersonic Streams, AIAA 2002-4277. (2002).
[2] R.S. Fry, A Century of Ramjet Propulsion Technology Evolution, J. Propuls. Power. 20 (2004) 27–58. https://doi.org/10.2514/1.9178.
[3] K. Ambe Verma, K. Murari Pandey, M. Ray, K. Kumar Sharma, Effect of transverse fuel injection system on combustion efficiency in scramjet combustor, Energy. 218 (2021). https://doi.org/10.1016/j.energy.2020.119511.
[4] S.H. Won, I.S. Jeung, B. Parent, J.Y. Choi, Numerical investigation of transverse hydrogen jet into supersonic crossflow using detached-eddy simulation, AIAA J. 48 (2010) 1047–1058. https://doi.org/10.2514/1.41165.
[5] E. Erdem, K. Kontis, Numerical and experimental investigation of transverse injection flows, Shock Waves. 20 (2010) 103–118. https://doi.org/10.1007/s00193-010-0247-1.
[6] Y. Zhang, W. Liu, B. Wang, Effects of oblique and transverse injection on the characteristics of jet in supersonic crossflow, Acta Astronaut. 115 (2015) 356–366. https://doi.org/10.1016/j.actaastro.2015.06.004.
[7] W. Huang, Transverse jet in supersonic crossflows, Aerosp. Sci. Technol. 50 (2016) 183–195. https://doi.org/10.1016/j.ast.2016.01.001.
[8] A. Anazadehsayed, M. Barzegar Gerdroodbary, Y. Amini, R. Moradi, Mixing augmentation of transverse hydrogen jet by injection of micro air jets in supersonic crossflow, Acta Astronaut. 137 (2017) 403–414. https://doi.org/10.1016/j.actaastro.2017.05.007.
[9] S. Jeyakumar, S.M. Assis, K. Jayaraman, Experimental study on the characteristics of axisymmetric cavity actuated supersonic flow, Proc. Inst. Mech. Eng. Part G J. Aerosp. Eng. 231 (2017) 2570–2577. https://doi.org/10.1177/0954410016667149.
[10] S.M. Assis, S. Jeyakumar, K. Jayaraman, The Effect of Transverse Injection Upstream of an Axisymmetric Aft Wall Angled Cavity in a Supersonic Flow Field, in: J. Phys. Conf. Ser., 2019. https://doi.org/10.1088/1742-6596/1276/1/012019.

[11] S. Jeyakumar, K.A. Yuvaraj, K. Jayaraman, F. Cardona, M.T.H. Sultan, Effect of cavity fore wall modifications in supersonic flow, in: IOP Conf. Ser. Mater. Sci. Eng., 2016. https://doi.org/10.1088/1757-899X/152/1/012002.
[12] S. Jeyakumar, V. Venkateshwaran, N. Surjith, A.K. Raja, G.S. Samy, Experimental investigations on aft ramp cavities with fore wall modifications in scramjet combustors, 2017. https://doi.org/10.1007/978-81-322-2743-4_114.
[13] S. Jeyakumar, K. Jayaraman, Effect of finite width cavity in axisymmetric supersonic flow field, Proc. Inst. Mech. Eng. Part G J. Aerosp. Eng. 232 (2018) 180–184. https://doi.org/10.1177/0954410016674036.
[14] S. Jeyakumar, S.M. Assis, K. Jayaraman, Effect of Axisymmetric Aft Wall Angle Cavity in Supersonic Flow Field, Int. J. Turbo Jet Engines. 35 (2018) 29–34. https://doi.org/10.1515/tjj-2016-0027.
[15] S. Jeyakumar, P. Balachandran, S. Indira, Experimental Investigations on Supersonic Stream Past Axisymmetric Cavities, J. Propuls. Power. 22 (2006) 1141–1144. https://doi.org/10.2514/1.21024.
[16] K. Wu, P. Zhang, W. Yao, X. Fan, Computational realization of multiple flame stabilization modes in DLR strut-injection hydrogen supersonic combustor, Proc. Combust. Inst. 37 (2019) 3685–3692. https://doi.org/10.1016/j.proci.2018.07.097.
[17] C.N.R. Chung-jen Tam, Kuang-Yu Hsu, Mark R. Gruber, Fuel / Air Mixing Characteristics of Strut Injections for Scramjet Combustor Applications, AIAA Pap. 2008-6925. (2008).
[18] L. Suneetha, P. Randive, K.M. Pandey, Numerical investigation on influence of diamond shaped strut on the performance of a scramjet combustor, Int. J. Hydrogen Energy. 44 (2019) 6949–6964. https://doi.org/10.1016/j.ijhydene.2019.01.187.
[19] K. Kumaran, P.R. Behera, V. Babu, Numerical Investigation of the Supersonic Combustion of Kerosene in a Strut-Based Combustor, J. Propuls. Power. 26 (2010) 1084–1091. https://doi.org/10.2514/1.46965.
[20] G. Choubey, K.M. Pandey, Effect of parametric variation of strut layout and position on the performance of a typical two-strut based scramjet combustor, Int. J. Hydrogen Energy. 42 (2017) 10485–10500. https://doi.org/10.1016/j.ijhydene.2017.03.014.
[21] C. Li, X. Chen, Y. Li, O. Musa, L. Zhu, Numerical investigation on the performance of scramjet combustor with a novel strut configuration, Appl. Therm. Eng. 159 (2019) 113894. https://doi.org/10.1016/j.applthermaleng.2019.113894.
[22] L. Suneetha, P. Randive, K.M. Pandey, Numerical investigation on implication of dual cavity on combustion characteristics in strut based scramjet combustor, Int. J. Hydrogen Energy. 44 (2019) 32080–32094. https://doi.org/10.1016/j.ijhydene.2019.10.064.
[23] J. Miao, Y. Fan, T. Liu, Influence of strut on cavity at subsonic speeds: Ignition characteristics, Proc. Inst. Mech. Eng. Part G J. Aerosp. Eng. 0 (2020) 1–11. https://doi.org/10.1177/0954410020904832.
[24] Y. Zong, W. Bao, J. Chang, J. Hu, Q. Yang, J. Song, M. Wu, Effect of fuel injection allocation on the combustion characteristics of a cavity-strut model scramjet, J. Aerosp. Eng. 28 (2015) 1–8. https://doi.org/10.1061/(ASCE)AS.1943-5525.0000374.
[25] K.-Y. Hsu, C.D. Carter, M.R. Gruber, T. Barhorst, S. Smith, Experimental Study of Cavity-Strut Combustion in Supersonic Flow, J. Propuls. Power. 26 (2010) 1237–1246. https://doi.org/10.2514/1.45767.
[26] L. Suneetha, P. Randive, K.M. Pandey, Numerical investigation on mixing behavior of fuels in reacting and non-reacting flow condition of a cavity-strut based scramjet combustor, Int. J. Hydrogen Energy. 44 (2019) 16718–16734. https://doi.org/10.1016/j.ijhydene.2019.04.262.
[27] G. Choubey, K.M. Pandey, Effect of different wall injection schemes on the flow-field of hydrogen fuelled strut-based scramjet combustor, Acta Astronaut. 145 (2018) 93–104. https://doi.org/10.1016/j.actaastro.2018.01.034.
[28] W. Waidmann, F. Alff, U. Brummund, M. Bohm, W. Clauss, M. Oschwald, Experimental

Investigation of the Combustion Process in a Supersonic Combustion Ramjet (Scramjet), Hardthausen, Ger. DLR Inst. Chem. 470 Propuls. Eng. (1994).
[29] M. Oevermann, Numerical investigation of turbulent hydrogen combustion in a SCRAMJET using flamelet modeling, Aerosp. Sci. Technol. 4 (2000) 463–480. https://doi.org/10.1016/S1270-9638(00)01070-1.
[30] O.R. Kummitha, K.M. Pandey, R. Gupta, Numerical analysis of hydrogen fueled scramjet combustor with innovative designs of strut injector, Int. J. Hydrogen Energy. 45 (2020) 13659–13671. https://doi.org/10.1016/j.ijhydene.2018.04.067.
[31] K. Kumaran, V. Babu, Investigation of the effect of chemistry models on the numerical predictions of the supersonic combustion of hydrogen, Combust. Flame. 156 (2009) 826–841. https://doi.org/10.1016/j.combustflame.2009.01.008.
[32] P. Gerlinger, D. Br-uacute, Ggemann, Numerical Investigation of Hydrogen Strut Injections into Supersonic Airflows, J. Propuls. Power. 16 (2000) 22–28. https://doi.org/10.2514/2.5559.
[33] W. Huang, Z.G. Wang, S. Bin Luo, J. Liu, Parametric effects on the combustion flow field of a typical strut-based scramjet combustor, Chinese Sci. Bull. 56 (2011) 3871–3877. https://doi.org/10.1007/s11434-011-4823-2.
[34] G. Choubey, K.M. Pandey, Effect of variation of angle of attack on the performance of two-strut scramjet combustor, Int. J. Hydrogen Energy. 41 (2016) 11455–11470. https://doi.org/10.1016/j.ijhydene.2016.04.048.
[35] S. Kumar, S. Das, S. Sheelam, Application of CFD and the Kriging method for optimizing the performance of a generic scramjet combustor, Acta Astronaut. 101 (2014) 111–119. https://doi.org/10.1016/j.actaastro.2014.04.003.
[36] M.C. Banica, T. Scheuermann, J. Chun, B. Weigand, J. Von Wolfersdorf, Numerical Study of Supersonic Combustion Processes with Central Strut Injection, J. Propuls. Power. 26 (2010) 869–874. https://doi.org/10.2514/1.43599.
[37] S. Aravind, R. Kumar, Supersonic combustion of hydrogen using an improved strut injection scheme, Int. J. Hydrogen Energy. 44 (2019) 6257–6270. https://doi.org/10.1016/j.ijhydene.2019.01.064.
[38] W. Huang, L. Yan, Numerical investigation on the ram-scram transition mechanism in a strut-based dual-mode scramjet combustor, Int. J. Hydrogen Energy. 41 (2016) 4799–4807. https://doi.org/10.1016/j.ijhydene.2016.01.062.
[39] Wu, K., Zhang, P., Yao, W. and Fan, X., Numerical Investigation on Flame Stabilization in DLR Hydrogen Supersonic Combustor with Strut Injection, Combust. Sci. Technol. 189 (2017), 2154–2179.
[40] Athithan, A. A., Jeyakumar, S., Sczygiol, N., Urbanski, M., & Hariharasudan, A., The Combustion Characteristics of Double Ramps in a Strut-Based Scramjet Combustor, Energies, 14(4), (2021), 831. https://doi.org/10.3390/en14040831.